*Supporting information*

---

# Photoactive Silicon Surfaces Functionalized with High-Quality and Redox-Active Platinum Diimine Complexes Monolayers

Bruno Fabre[1,*], Franck Camerel[1,*] and Soraya Ababou-Girard[2]

[1] *Univ Rennes, CNRS, ISCR (Institut des Sciences Chimiques de Rennes)-UMR6226, F-35000 Rennes, France*

[2] *Univ Rennes, CNRS, IPR (Institut de Physique de Rennes)-UMR 6251, F-35000 Rennes, France*

*E-mail: bruno.fabre@univ-rennes1.fr; franck.camerel@univ-rennes1.fr*

## Table of Contents

**Instrumentation.**

300 ($^{1}$H) and 75.5 MHz ($^{13}$C) NMR spectra were recorded on Bruker Avance 300 spectrometer at room temperature using perdeuterated solvents as internal standards. FT-IR spectra were recorded using a Bruker VERTEX 70 spectrometer equipped with an ATR apparatus. Elemental analyses were performed by the Service de Microanalyse, Centre régional de mesures physiques de l'Ouest (CRMPO), Rennes, France. Mass spectra were recorded with a MALDI-TOF Microflex LT Bruker. UV-Vis spectra were recorded using a Shimadzu UV-3600 plus UV-vis-NIR spectrophotometer.

Photothermal studies were performed by irradiating 2 mL of solutions with a 808 nm continuous semiconductor laser with an optical fiber (105 µm / 0.22) (Changchun New Industries Optoelectronics) through a quartz cuvette for 10 min. The laser power density could be adjusted externally (0-10 W). The power input to the solution was independently calibrated using an optical power meter through a 1 cm diameter spherical opening mask placed in front of the cuvette. A thermocouple with an accuracy of ± 0.1 °C connected to STANDARD ST-8891E Moineau instruments thermometer was inserted into the solution. The thermocouple was inserted at such a position that direct irradiation from the laser was avoided. The temperature was measured every 1s. The photothermal efficiency (η) value was calculated according to the following equation described by Roper and al. based on the energy balance of the system.[1]

Differential scanning calorimetry (DSC) was carried out by using NETZSCH DSC 200 F3 instrument equipped with an intracooler. DSC traces were measured at 10 °C/min down to -25 °C.

Optical microscopy investigations were performed on a Nikon H600L polarizing microscope equipped with a Linkam "liquid crystal pro system" hotstage LTS420. The microscope is also equipped with a UV irradiation source (Hg Lamp, λ = 340-380 nm) and an ocean optic USB 2000+ UV-Vis-NIR spectrophotometer based on CCD detection technology.

XPS measurements were performed with an Mg Kalpha (hv) 1254 eV X-ray source, using a VSW HA100 photoelectron spectrometer with a hemispherical photoelectron analyzer, working at an energy pass of 20 eV for survey and resolved spectra. The experimental resolution was 1.0 eV.

Cyclic voltammetry measurements were performed with an Autolab electrochemical analyzer (PGSTAT 30 potentiostat/galvanostat from Eco Chemie B.V.) equipped with the GPES and FRA softwares in a home-made three-electrode glass cell. For measurements in solution, the working electrode was a 3 mm-diameter glassy carbon rod. For measurements in supported phase, the working electrode, modified Si(111), was pressed against an opening in the cell side using a Teflon circular piece and a FETFE (Aldrich) O-ring seal. An ohmic contact was made on the previously polished rear side of

the sample by applying a drop of In-Ga eutectic (Alfa-Aesar, 99.99%). A steel piece was dropped on the eutectic-coated sample and then the assembly was screwed to the cell using a plastic cap screw. The electrochemically active area of the Si(111) surface (namely 0.38 $cm^2$) was estimated by measuring the charge under the voltammetric peak corresponding to the ferrocene oxidation on Si(111)-H and compared to that obtained with a 1 $cm^2$-Pt electrode under the same conditions. For both measurements, the counter electrode was a carbon rod and the system $10^{-2}$ M $Ag^+$ | Ag in acetonitrile was used as the reference electrode. All reported potentials are referred to KCl-saturated calomel electrode (uncertainty ± 5 mV) using the reversible ferrocenium/ferrocene couple as the redox probe. Tetra-n-butylammonium hexafluorophosphate $Bu_4NPF_6$ or perchlorate $Bu_4NClO_4$ (Fluka, puriss, electrochemical grade) was used at 0.2 or 0.1 mol $L^{-1}$ as supporting electrolyte in methylene chloride or acetonitrile for the homogeneous or heterogeneous phase, respectively. The electrolytic medium was dried over activated, neutral alumina (Merck) for 30 min, under stirring and under argon. About 20 mL of this solution was transferred with a syringe into the electrochemical cell prior to experiments. All electrochemical measurements were carried out inside a home-made Faraday cage, at room temperature (20 ± 2 ºC) under constant argon gas flow. For measurements at modified photoelectrodes, the light was provided by a solar simulator with a fluence of 100 mW $cm^{-2}$ (LS0106, LOT Quantum Design) equipped with a AM 1.5G and red (Edmund Optics) filters. The Ohmic drop was determined before each experiment by measuring the impedance of the system at 100 kHz and it was found to be around 440-490 Ω in ($CH_3CN$ + 0.1M $Bu_4NClO_4$) electrolytic medium, depending on the type of the tested photoelectrode (the area was always kept constant at 0.38 $cm^2$). The experimental potential scale $E_{exp}$ was converted to Ohmic-drop corrected potential scale $E_{RI}$ by using $E_{exp} = E_{RI} + (R \times j \times A)$ where $R$ is the resistance determined from impedance measurements, $j$ is the current density (in A $cm^{-2}$) and $A$ is the area of the modified silicon surface (0.38 $cm^2$).

AFM measurements were recorded in Tapping mode with a microscope from Asylum Research Cypher using monocrystal silicon tips from NT-MDT (resonance frequency, 330 kHz; JA_HR_DCP probe series).

Spectroscopic ellipsometry experiments were performed in the range 300-800 nm at three incidence angles of 65, 70 and 75°, using a Horiba ellipsometer, and analyzed with a two-layer (Si + alkyl) model.

**Density Functional Theory (DFT) Calculations.**

DFT[2] calculations of the optimized geometrical structures of the silicon-bound Pt complexes were performed with the hybrid Becke-3 parameter exchange functional[3] and the Lee-Yang-Parr nonlocal

correlation functional[4] (B3LYP) implemented in the *Gaussian 09 (Revision B.01)* program suite[5] using the pseudo-potentials LANL2DZ with the default convergence criteria implemented in the program. Calculations were carried out on the OCCIGEN calculator of the Centre Informatique National de l'Enseignement Supérieur (CINES (Montpellier) under project 2021-A0100805032). Figures S20 and S21 were generated with GaussView 5.0 and Chem3D.

**Synthesis.**

[2,2'-bipyridine]-4,4'-dicarboxylic acid, [6] 2,2-dibutyl-5,6-dihydro-1,3,2-dithiastannolo[4,5-b][1,4]dithiin[7] and $PtCl_2(DMSO)_2$[8] were synthesized as previously described. All the other reagents were purchased from commercial sources and used as received. All synthetic manipulations were performed under an inert and dry nitrogen atmosphere using standard techniques. The reactions were followed by Thin Layer Chromatography (TLC) plates, revealed with a UV-lamp at 254 nm or iodine. Aluminium oxide 90 standardized from Merck KGaA was used for chromatographic separations.

**di(dec-9-en-1-yl) [2,2'-bipyridine]-4,4'-dicarboxylate**

[2,2'-bipyridine]-4,4'-dicarboxylic acid (0.172 g, 0.7 mmol) was first refluxed 4 h in 10 mL freshly distilled $SOCl_2$ at 90 °C under $N_2$ with 1 drop of $Et_3N$. After removal of the excess $SOCl_2$ and drying, the residue was dissolved in 20 mL of dry $CH_2Cl_2$ with 9-decen-1-ol (0.275 g, 1.75 mmol) and $Et_3N$ (0.3 mL, 2.2 mmol) were added. The mixture was stirred at room temperature under $N_2$ for 48h. The organic phase was washed with water (3x40 mL) and dried over $MgSO_4$. The product was purified by column chromatography on alumina using a gradient of eluents from pure petroleum ether to pure dichloromethane. After recrystallization in a $CH_2Cl_2$/MeOH mixture, the product was isolated as a white powder in 79 % yield (0.29 g). $^1$H NMR (300 MHz, $CDCl_3$) δ 8.95 (s, 2H, $CH_{arom}$), 8.86 (dd, J = 5.0, 0.9 Hz, 2H, $CH_{arom}$), 7.90 (dd, J = 5.0, 1.6 Hz, 2H, $CH_{arom}$), 5.81 (ddt, J = 17.0, 10.2, 6.7 Hz, 2H, **CH**=$CH_2$), 5.06 – 4.87 (m, 4H, CH=**$CH_2$**), 4.39 (t, J = 6.8 Hz, 4H, $OCH_2$), 2.11 – 1.96 (m, 4H, $CH_2$), 1.90 – 1.72 (m, 4H, $CH_2$), 1.53 – 1.23 (m, 20H, $CH_2$). $^{13}$C NMR (75 MHz, $CDCl_3$) δ 165.40 (C=O), 156.76 (Cq), 150.24 (CH), 139.28 (=CH), 139.18 (Cq), 123.35 (CH), 120.74 (CH), 114.33 (=$CH_2$), 66.20 ($OCH_2$), 33.91 ($CH_2$), 29.48 ($CH_2$), 29.35 ($CH_2$), 29.17 ($CH_2$), 29.04 ($CH_2$), 28.78 ($CH_2$), 26.09 ($CH_2$). UV-vis [$CH_2Cl_2$, λmax (nm) (ε ($M^{-1}.cm^{-1}$))]: 242 (10400), 300 (11300). MALDI-TOF-MS: m/z = 521.4 ($[M+H]^+$). Anal. Calc. for $C_{32}H_{44}N_2O_4$, 1/12 $CH_2Cl_2$ (%): C 73.01, H 8.44, N 5.31. Found (%): C 73.05, H 8.31, N 5.28.

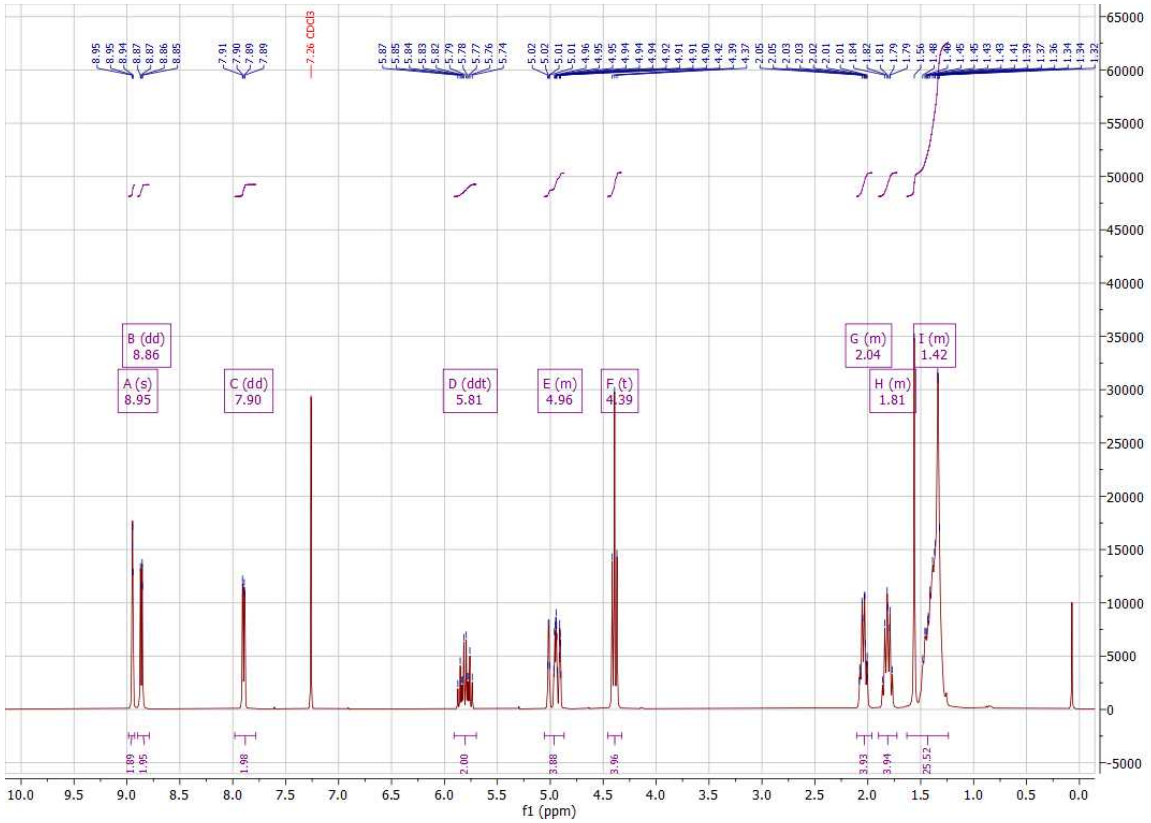


**Figure S1.** $^{1}H$ NMR spectra of the bipyridine ligand in $CDCl_3$.

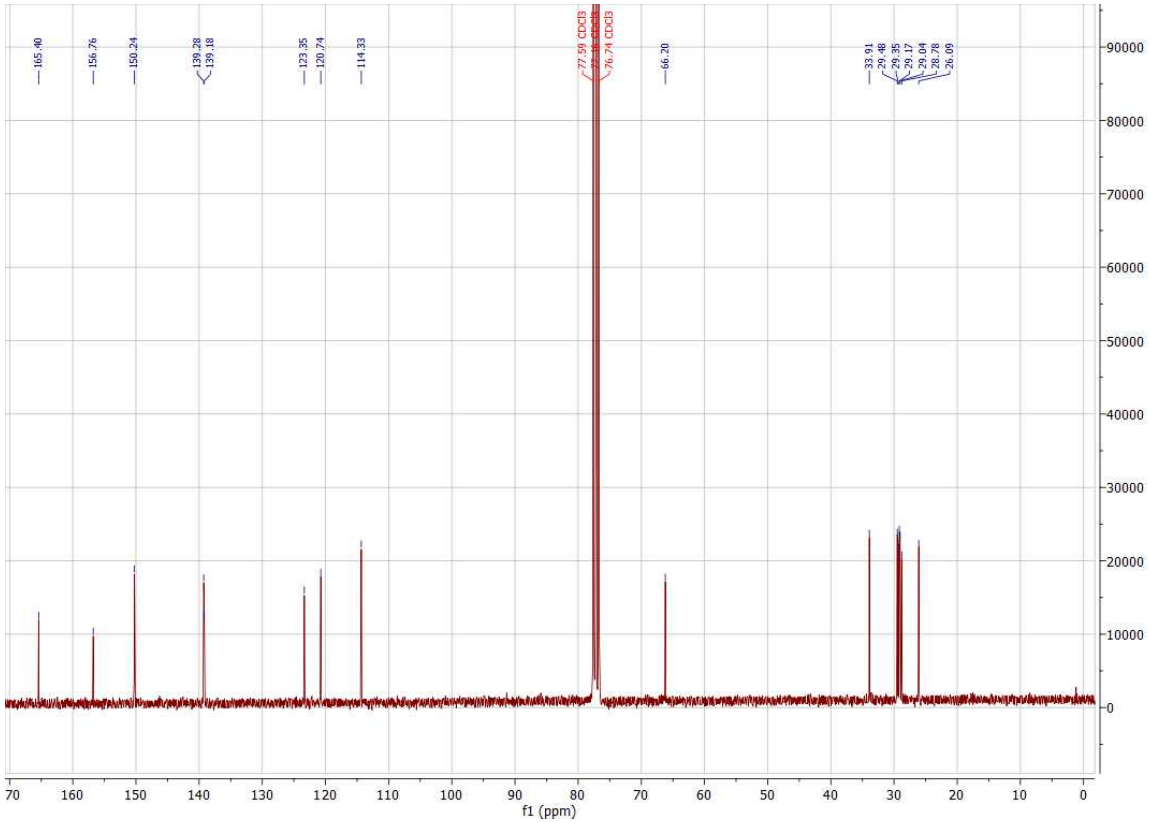


**Figure S2.** $^{13}C$ NMR spectra of the bipyridine ligand in $CDCl_3$.

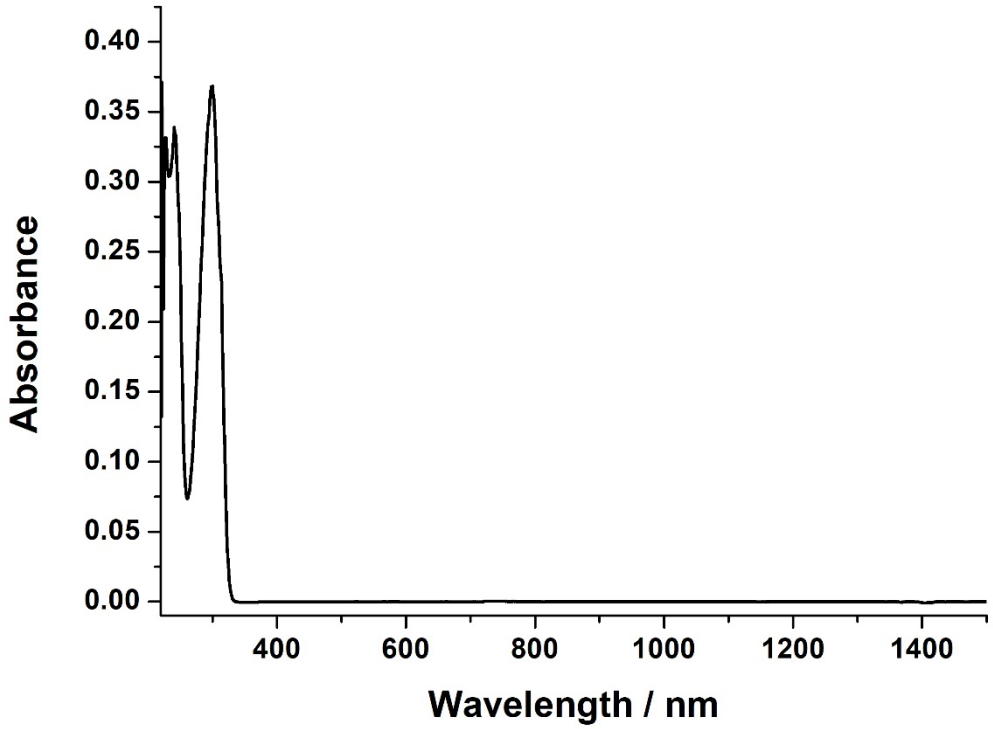


**Figure S3.** UV-vis-NIR spectrum of the bipyridine ligand in $CH_2Cl_2$ (C= 3.26 x $10^{-5}$ M).

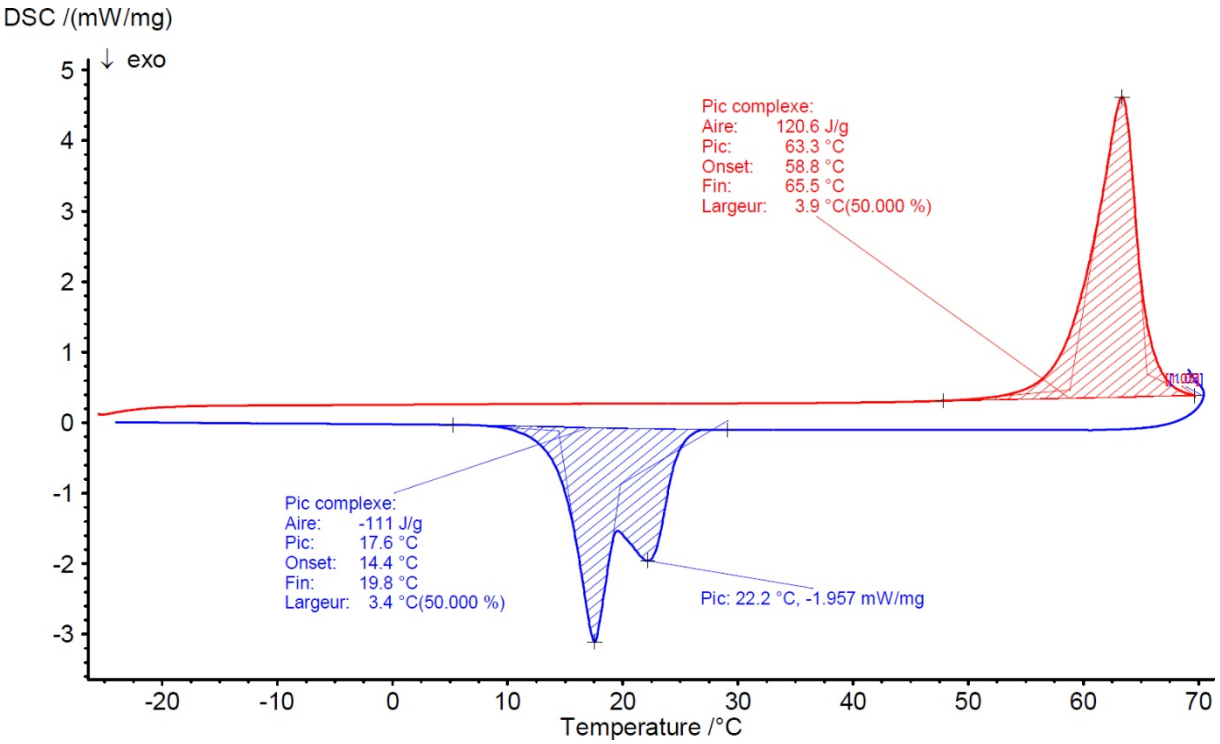


**Figure S4.** DSC curves of the bipyridine ligand (red: 2nd heating curve, blue: 1st cooling curve, heating and cooling rate: 10 °C / min).

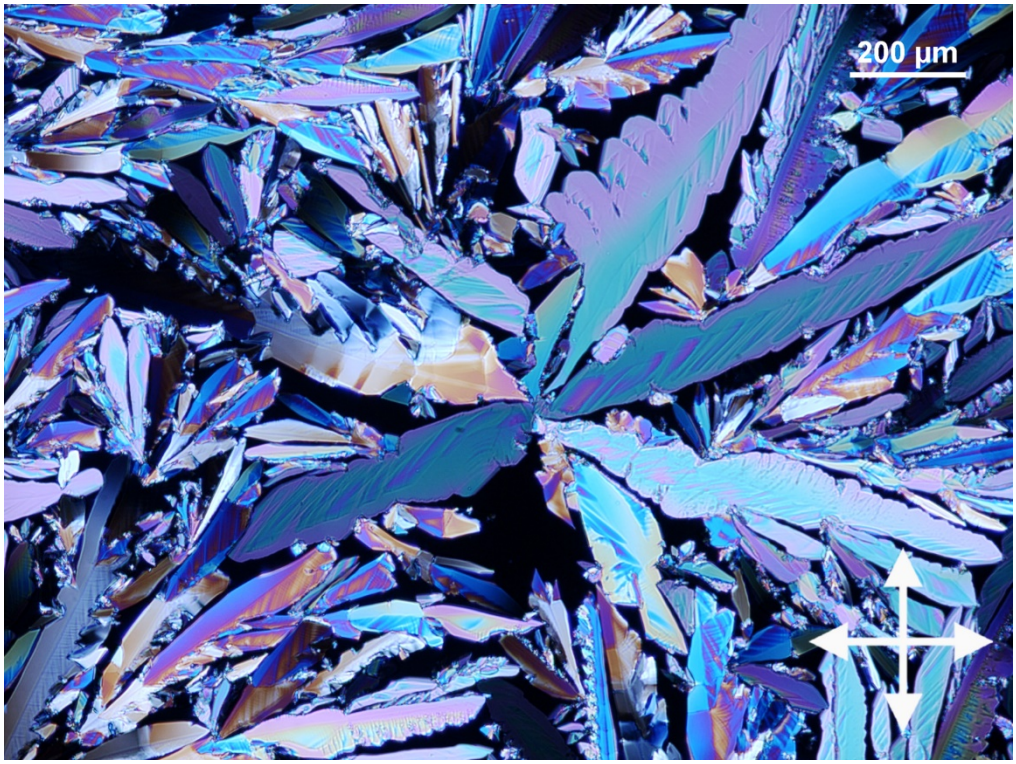


**Figure S5.** Polarized optical microscopy image of the bipyridine ligand at 25 °C after cooling from the isotropic phase (crossed polarisers are represented by the white cross in the corner).

**di(dec-9-en-1-yl) [2,2'-bipyridine]-4,4'-dicarboxylate dichloro platinum ($PtCl_2$) complex**

di(dec-9-en-1-yl) [2,2'-bipyridine]-4,4'-dicarboxylate Ligand (0.29 g, 0.57 mmol) was dissolved in 10 mL dry THF in a Schlenk flask with 1 eq. of $PtCl_2(DMSO)_2$ (0.24 g, 0.57 mmol) and the reaction mixture was then heated at 40 °C for 48h under $N_2$. After removal of the solvent and purification by column chromatography on alumina gel using $CHCl_3$ as eluent, the product was isolated as a yellow-orange gel-like material in 81 % yield (0.36 g).

$^1$H NMR (300 MHz, $CDCl_3$) δ 9.56 (d, J = 6.0 Hz, 2H, $CH_{arom}$), 8.55 (d, J = 1.8 Hz, 2H, $CH_{arom}$), 7.99 (dd, J = 6.0, 1.7 Hz, 2H, $CH_{arom}$), 5.80 (ddt, J = 16.9, 10.2, 6.6 Hz, 2H, **CH**=$CH_2$), 5.17 – 4.81 (m, 4H, CH=**$CH_2$**), 4.44 (t, J = 6.9 Hz, 4H, $OCH_2$), 2.05 (q, J = 7.1 Hz, 4H, $CH_2$), 1.84 (q, J = 7.1 Hz, 4H, $CH_2$), 1.51 – 1.18 (m, 20H, $CH_2$). $^{13}$C NMR (75 MHz, $CDCl_3$) δ 163.16 (C=O), 157.64 (Cq), 149.93 (CH), 140.51 (Cq), 139.19 (=CH), 126.84 (CH), 123.48 (CH), 114.32 (=$CH_2$), 67.37 ($OCH_2$), 33.86 ($CH_2$), 29.78 ($CH_2$), 29.44 ($CH_2$), 29.29 ($CH_2$), 29.14 ($CH_2$), 28.98 ($CH_2$), 28.62 ($CH_2$), 25.97 ($CH_2$). UV-vis [$CH_2Cl_2$, λmax (nm), ε ($M^{-1}.cm^{-1}$)]: 301 (22650), 422 (4900). MALDI-TOF-MS: m/z = 750.2 (M+-Cl). Anal. Calc. for $C_{32}H_{44}Cl_2N_4O_6Pt$, 0.5 $C_6H_{14}$ (%): C 49.78, H 5.92, N 3.47. Found (%): C 49.93, H 5.90, N 3.44.

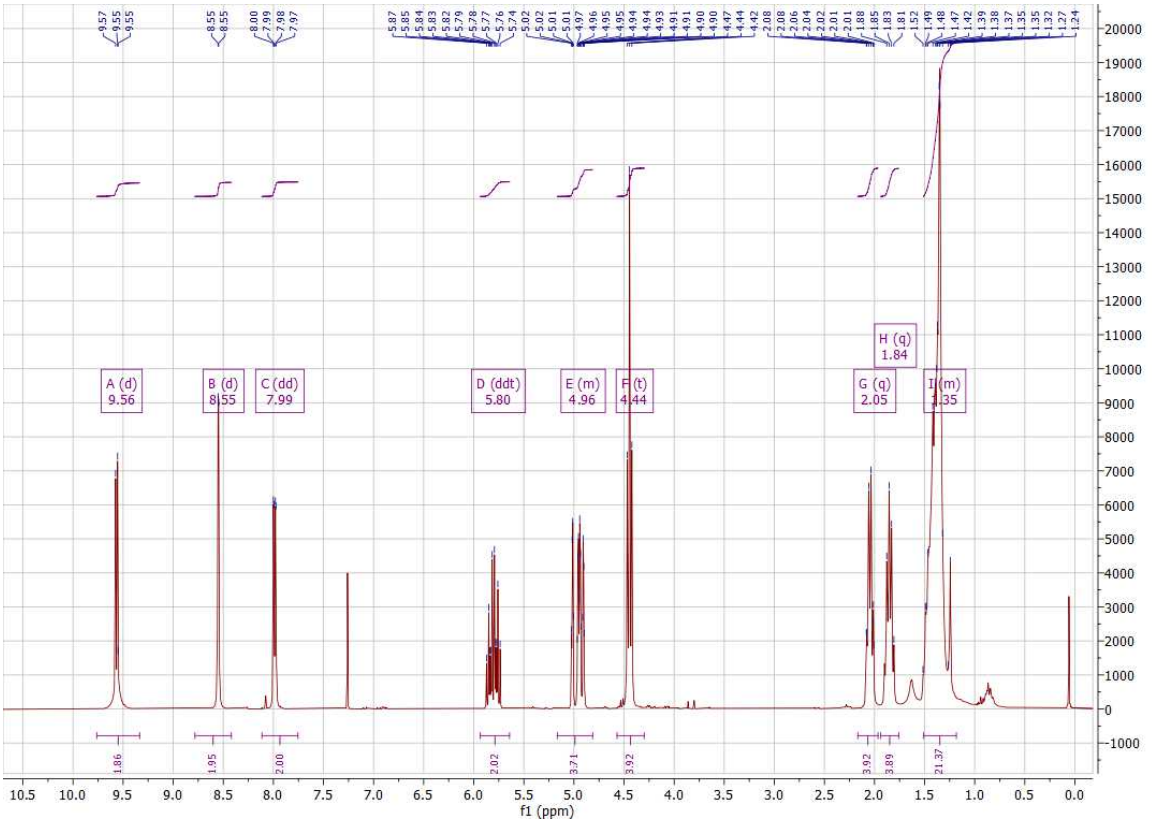


**Figure S6.** $^{1}$H NMR spectrum of the **$PtCl_2$** complex in $CDCl_3$.

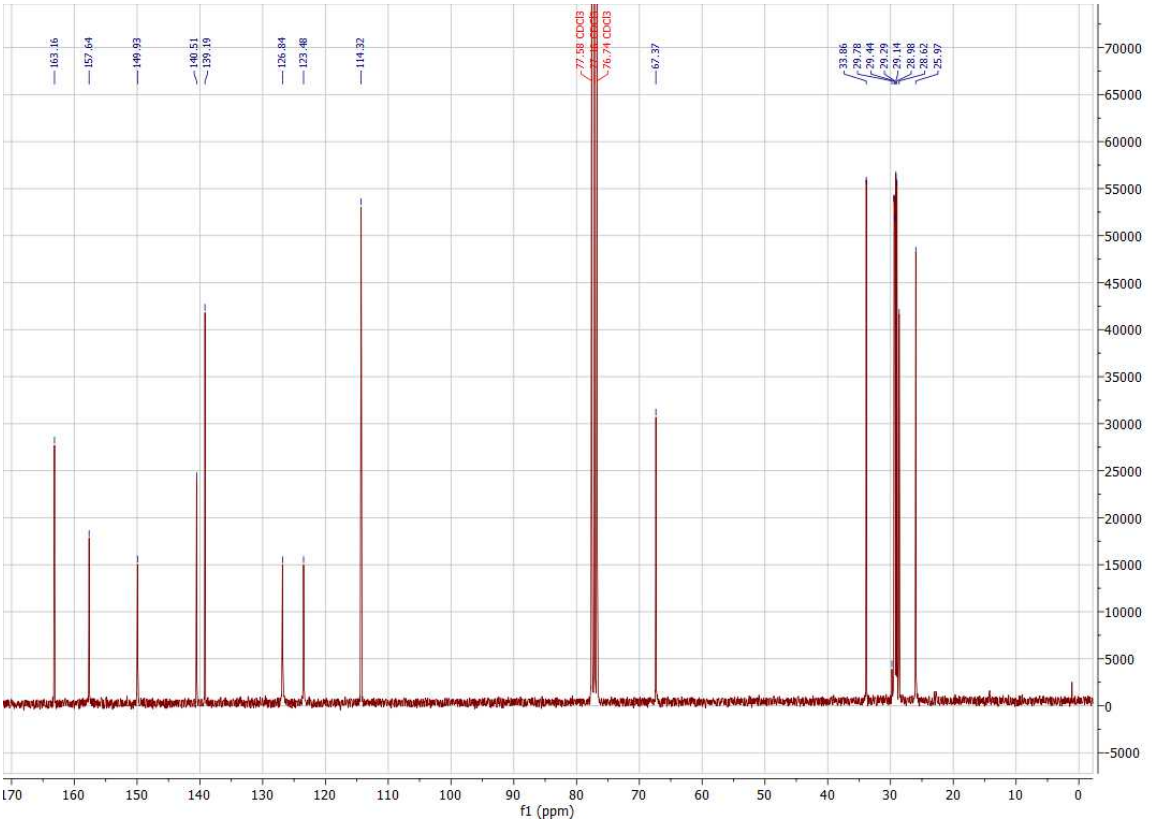


**Figure S7.** 13C NMR spectrum of the **$PtCl_2$** complex in $CDCl_3$.

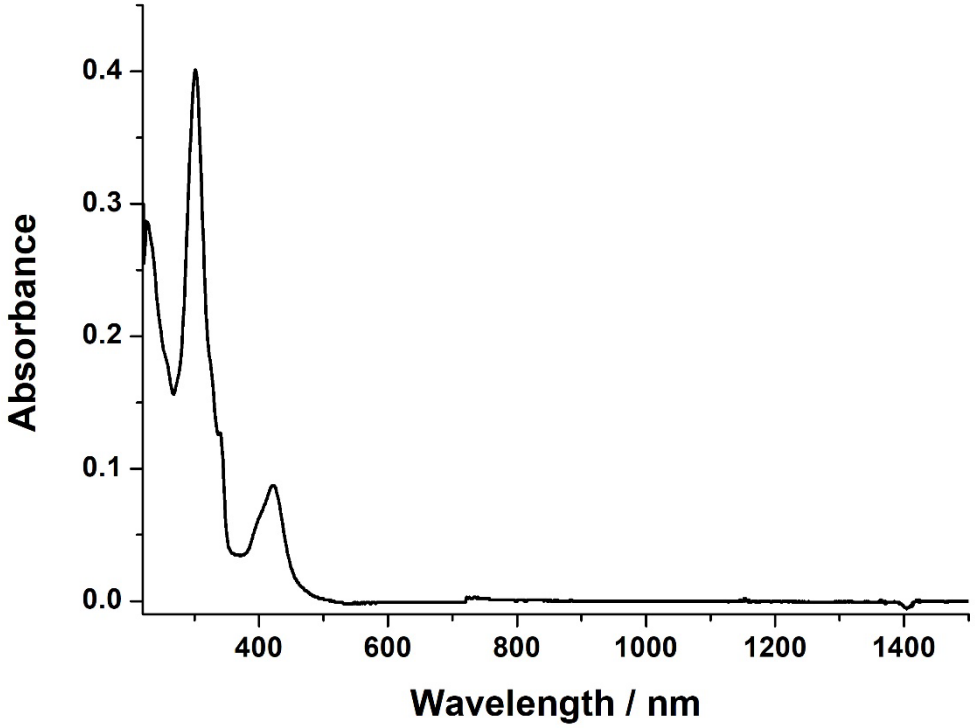


**Figure S8.** UV-vis-NIR spectrum of the **$PtCl_2$** complex in $CH_2Cl_2$ (C= 1.77 x $10^{-5}$ M).

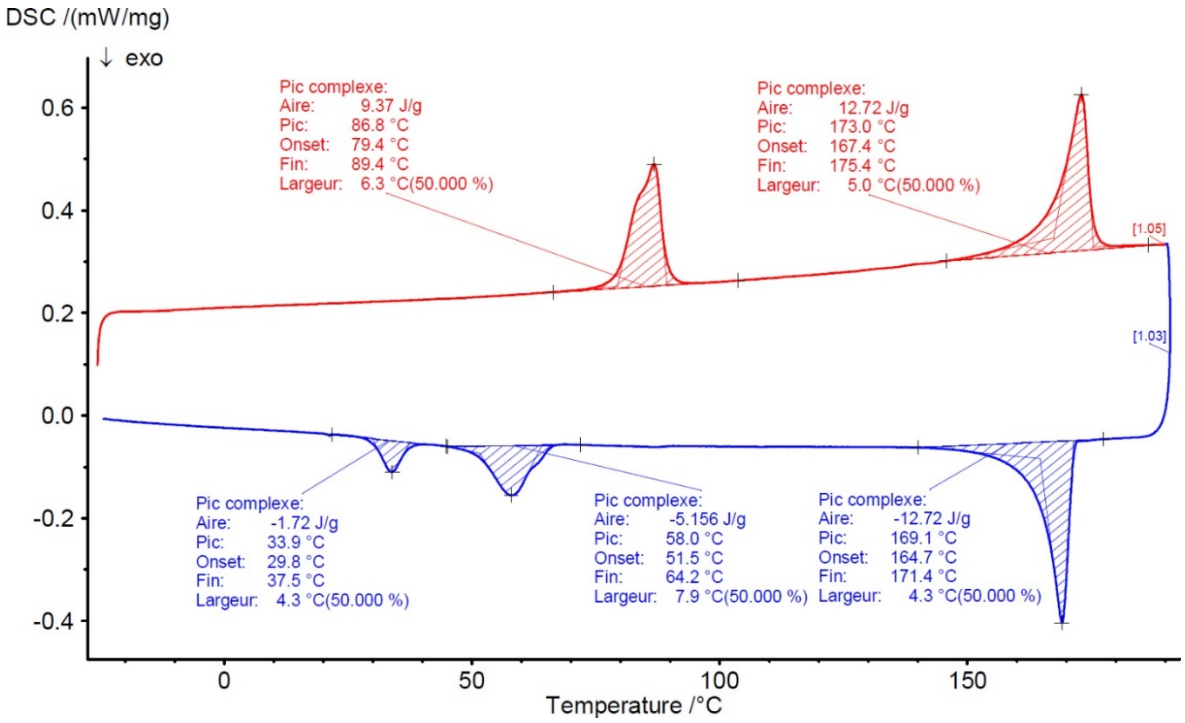


**Figure S9.** DSC curves of the **$PtCl_2$** complex (red: 2nd heating curve, blue: 1st cooling curve, heating and cooling rate: 10 °C / min).

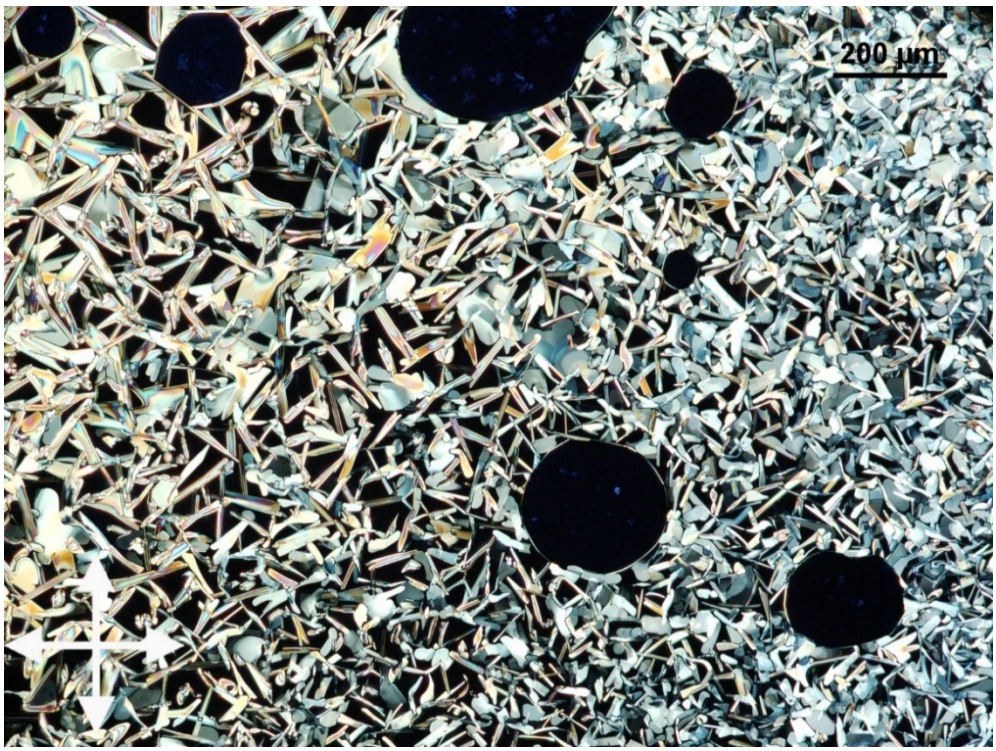


**Figure S10.** Polarized optical microscopy image of the **$PtCl_2$** complex at 140 °C after cooling from the isotropic phase (crossed polarisers are represented by the white cross in the corner).

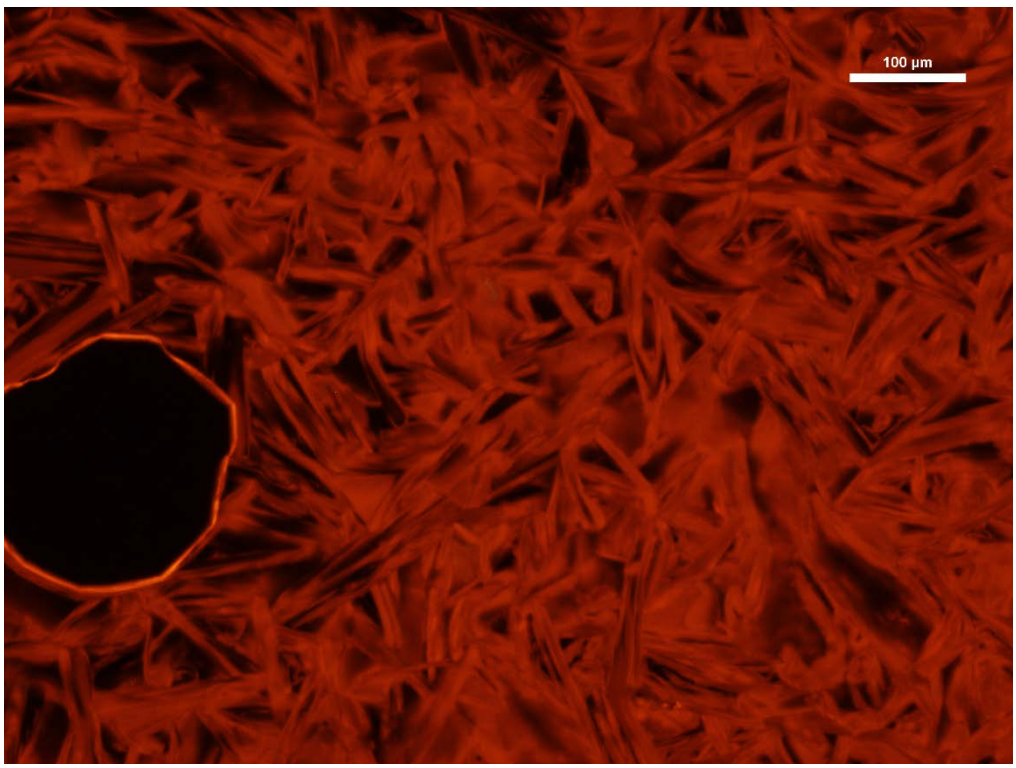


**Figure S11.** Microscopy image under UV irradiation ($\lambda_{ex}$ = 340-380 nm) of the **$PtCl_2$** complex at 60 °C after cooling from the isotropic phase.

**Diimine-dithiolene platinum (Ptdithiolene) complex**

The **$PtCl_2$** complex (0.26 g, 0.335 mmol) was dissolved in a mixture of acetone (10 mL) and THF (4 mL) and 1.1 equivalent of 2,2-Dibutyl-5,6-dihydro-1,3,2-dithiastannolo[4,5-b][1,4]dithiin (0.15 g, 0.37 mmol) was added. The reaction mixture was stirred at room temperature under $N_2$ atmosphere. After 4 days, solvent was evaporated and the product was purified by column chromatography on alumina gel using $CHCl_3$ as eluent. The compound was isolated as a green sticky powder in 70 % yield (0.21 g). $^1$H NMR (300 MHz, $CDCl_3$) δ 8.84 (d, J = 5.9 Hz, 2H, $CH_{arom}$), 8.50 (d, J = 1.8 Hz, 2H, $CH_{arom}$), 7.78 (dd, J = 5.9, 1.6 Hz, 2H, $CH_{arom}$), 5.82 (ddt, J = 16.9, 10.2, 6.6 Hz, 2H, **CH**=$CH_2$), 5.14 – 4.82 (m, 4H, CH=**$CH_2$**), 4.43 (t, J = 6.9 Hz, 4H, $OCH_2$), 2.94 (s, 4H, $SCH_2$ dithioligand), 2.07 (q, J = 7.1 Hz, 4H, $CH_2$), 1.86 (p, J = 6.9 Hz, 4H, $CH_2$), 1.63 – 1.15 (m, 20H, $CH_2$). $^{13}$C NMR (75 MHz, $CDCl_3$) δ 163.92 (C=O), 156.02 (Cq), 148.33 (CH), 139.24 (=CH), 138.54 (Cq), 126.85 (CH), 123.81 (CH), 114.38 (=$CH_2$), 66.90 ($OCH_2$), 33.92 ($CH_2$), 29.83 ($CH_2$), 29.53 ($CH_2$), 29.41 ($CH_2$), 29.22 ($CH_2$), 29.06 ($CH_2$), 28.77 ($CH_2$), 26.10 ($CH_2$). The ddt fragment is not visible on the $^{13}$C NMR spectrum. UV-vis [$CH_2Cl_2$, λmax (nm), ε ($M^{-1}.cm^{-1}$)]: 320 (43100), 366 (11150), 422 (5150), 512 (4800), 774 (15700). MALDI-TOF-MS: m/z = 895.2 ($M^+$). Anal. Calc. for $C_{36}H_{48}N_4O_4PtS_4$ (%): C 48.25, H 5.40, N 3.13, S 14.31. Found (%): C 48.01, H 5.37, N 2.99, S 14.41.

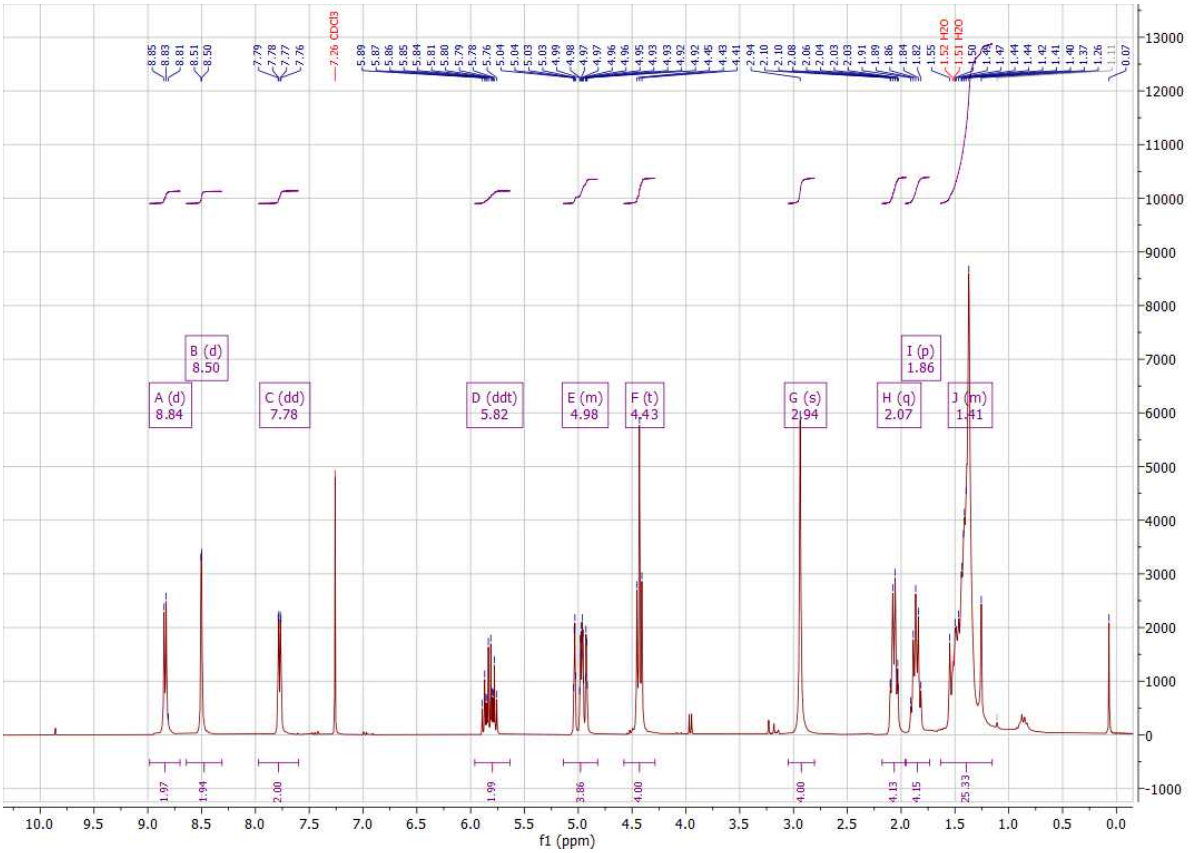


**Figure S12.** $^{1}$H NMR spectrum of the **Ptdithiolene** complex in $CDCl_3$.

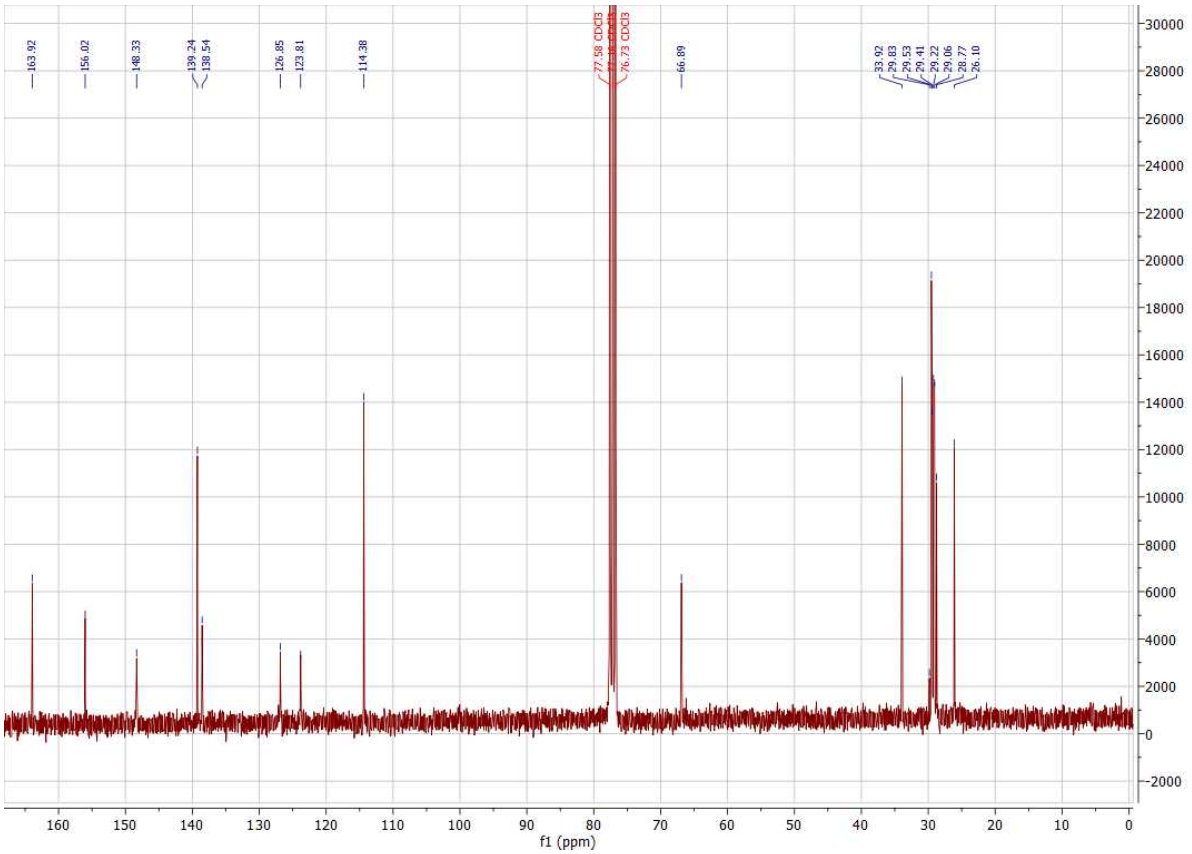


**Figure S13.** $^{13}$C NMR spectrum of the **Ptdithiolene** complex in $CDCl_3$.

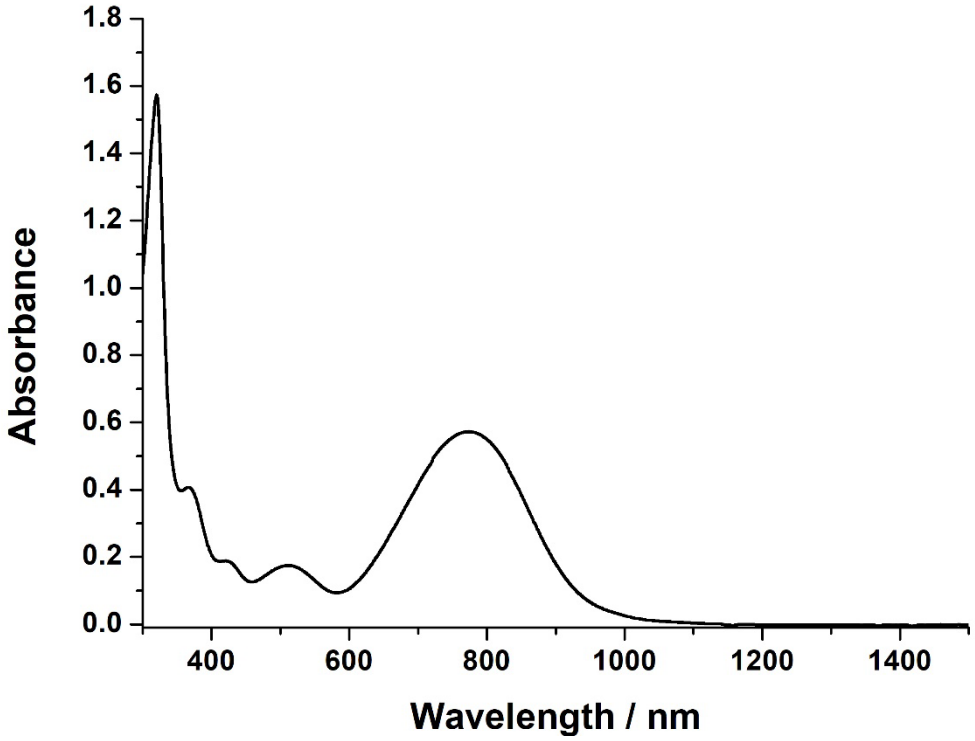


**Figure S14.** UV-vis-NIR spectrum of the **Ptdithiolene** complex in $CH_2Cl_2$ (C= 3.65 x $10^{-5}$ M).

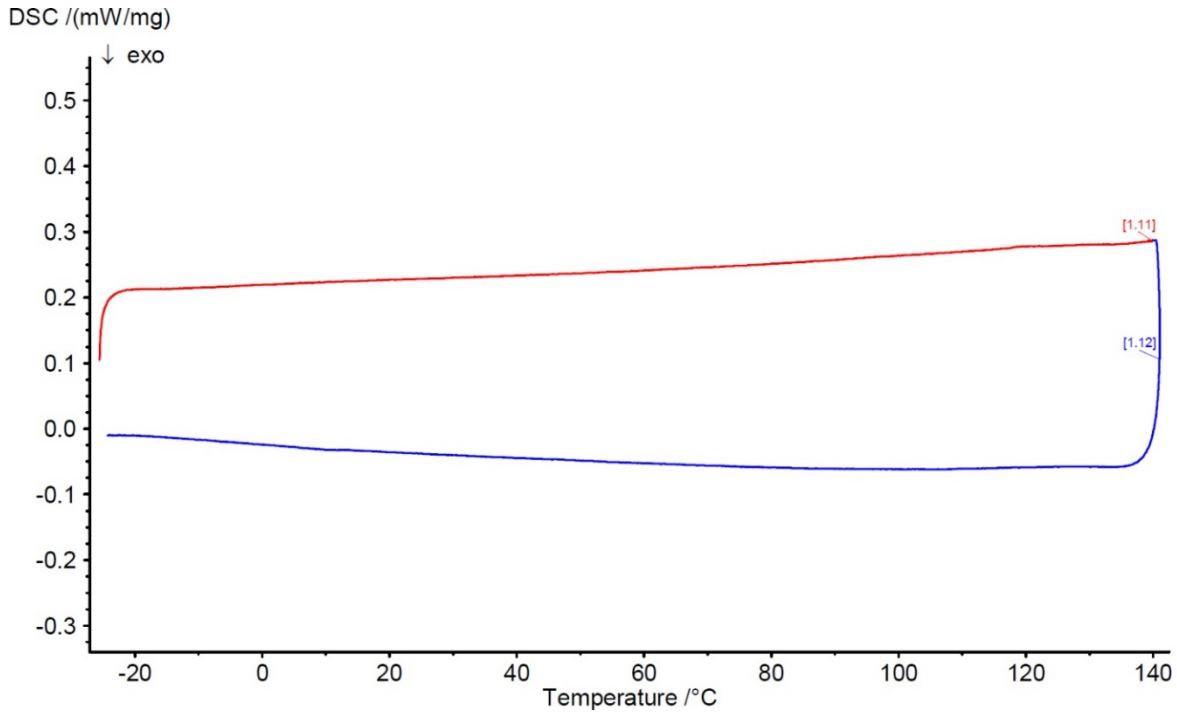


**Figure S15.** DSC curves of the **Ptdithiolene** complex (red: 2nd heating curve, blue: 1st cooling curve, heating and cooling rate: 10 °C / min).

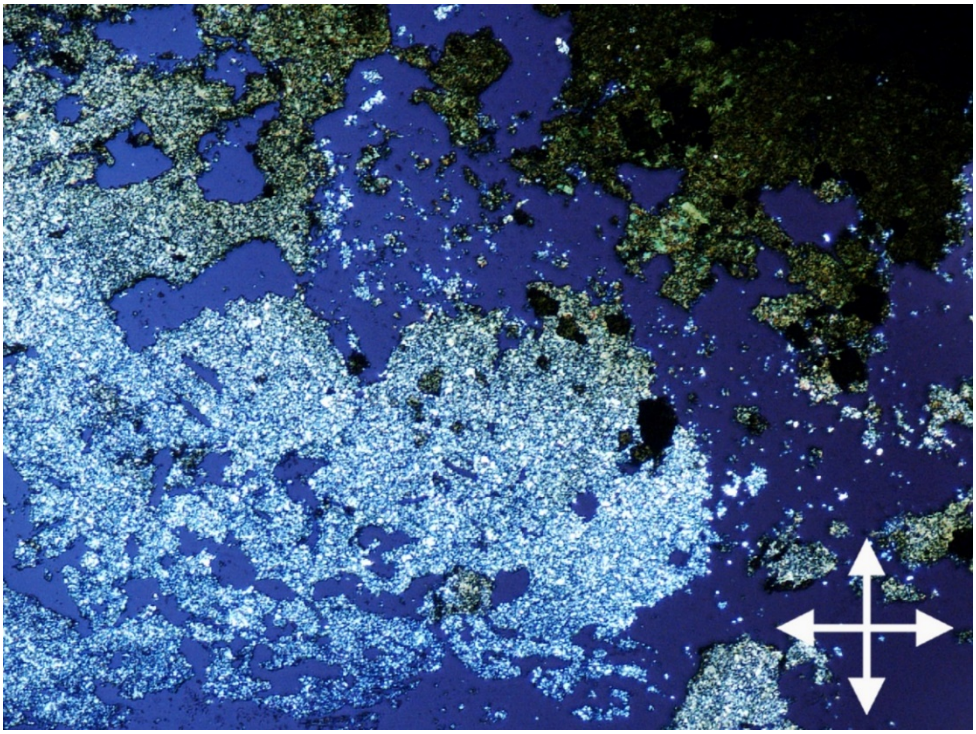

**Figure S16.** Polarized optical microscopy image of the **Ptdithiolene** complex at 140 °C in a birefringent gel state after gentle pressure on the cover glass slide (crossed polarisers are represented by the white cross in the corner).

**Preparation of Pt complex-modified *p*-type Si(111) surfaces**

Mesitylene (99%, extra-pure, from Acros) was passed through an activated, neutral alumina column, distilled over sodium under reduced pressure, and stored in the fridge under argon over $CaCl_2$ pellets. The chemicals used for cleaning and etching silicon wafer pieces (30% $H_2O_2$, 96-97% $H_2SO_4$, 50% HF and 40% $NH_4F$ solutions) were of VLSI semiconductor grade (Riedel-de-Haën). All Teflon vials used for cleaning of silicon were previously decontaminated in 3:1 v/v concentrated $H_2SO_4$/30% $H_2O_2$ at 100°C for 30 min, followed by copious rinsing with ultra-pure water.

***Caution**: The concentrated $H_2SO_4$:$H_2O_2$ (aq) piranha solution is very dangerous, particularly in contact with organic materials, and should be handled extremely carefully.*

All single side polished Si(111) samples (*p*-type, boron doped, 1-5 Ω cm, thickness = 525±25 $\mu$m, from Siltronix) were cut into 1.5 × ca. 4.0 $cm^2$ pieces from the same silicon wafer to ensure the maximum reproducibility of hydrogen-terminated and further molecular monolayer-modified surfaces. The sample was sonicated for 10 min successively in acetone (MOS semiconductor grade, Carlo Erba), ethanol (99.8%, VLSI semiconductor grade) and ultra-pure 18.2 MΩ cm water (Elga Purelab Classic UV,

Veolia). It was then cleaned in 3:1 v/v concentrated $H_2SO_4$/30% $H_2O_2$ at 100°C for 30 min, followed by copious rinsing with ultra-pure water. The surface was first etched in ca. 5-10% HF for 1 min, then in argon-degassed ppb grade 40% aqueous $NH_4F$ for 20 min at room temperature.[9] The $NH_4F$ solution was thoroughly degassed with argon for at least 1 h prior to the immersion of the piranha-treated surface. After etching, the hydrogen-terminated surface (Si-H) was rinsed with argon-saturated water, blown dry with argon, and transferred immediately into a Pyrex Schlenk tube containing the deoxygenated Pt complex ω-substituted by an alkene unit (dissolved in mesitylene at ca. 10 mM). The grafting solution was previously heated at 100°C for at least 1 h, then allowed to cool down to room temperature before introducing Si-H. Mesitylene was selected to dissolve the Pt complex since it has been demonstrated that the use of aromatic solvents with high boiling point was an efficient method for producing high-quality and well-ordered organic monolayers on silicon.[10] An aluminum foil was put around the glassware to avoid the possible photochemical degradation of the Pt complex. The hydrosilylation reaction was either thermally (110°C overnight or 180°C for 3 h) or UV activated (at 300 nm for 4 h) and the alkene solution was kept under a pressure of argon during the reaction. After the hydrosilylation reaction, the modified Si(111) surface was thoroughly rinsed with toluene (HPLC grade, from Fisher) and dichloromethane (RSE, electronic grade, from Carlo-Erba), then dried under argon.

The grafting of the Pt dithiolene complex on Si-H surfaces was performed using two approaches (Scheme 1). The first is based on the direct grafting of this complex from its precursor ω-substituted by an alkene unit (**Ptdithiolene**). The second is a two-step method and consists first of the hydrosilylation reaction of an alkene-substituted $PtCl_2$ complex (**$PtCl_2$**) with Si-H followed by the conversion of the $PtCl_2$ headgroup of the monolayer to the Pt-dithiolene complex using the following experimental conditions: introduction of the **$PtCl_2$**-modified surface into a deoxygenated solution of 5:1 v/v acetone/THF (5 mL) containing 10 mM of 2,2-dibutyl-5,6-dihydro-1,3,2-dithiastannolo[4,5-b][1,4]dithiin, reaction under argon at room temperature for 2 h, rinsing with acetone and dichloromethane, and drying under argon.

The grafting conditions were optimized in order to produce the Pt dithiolene-terminated monolayer with the highest Pt complex surface coverage, the lowest oxidation level of the underlying silicon surface, XPS and ellipsometric data consistent with the expected monolayer composition and thickness, respectively (Table S1). The optimal reaction conditions were as follows: two-step grafting reaction using 300 nm for 4 h for the first hydrosilylation step.

**Table S1.** Different experimental conditions used for the optimization of the grafting of the Pt dithiolene complex-terminated monolayer on Si-H. The optimal conditions are highlighted in green.

| Entry | Grafting | Conditions | Remarks |
|---|---|---|---|
| 1 | One-step | 180°C for 3 h | Grafting of a polymer film and degradation of the **Ptdithiolene** solution, no Si detected by XPS[a] |
| 2 | One-step | 110°C overnight | Grafting of a polymer film, no Si detected by XPS[a] |
| 3 | One-step | 300 nm for 4 h | Low surface coverage estimated by XPS (3 x $10^{13}$ atoms $cm^{-2}$, i.e. 0.04 Pt complex per surface silicon atom),[b] weakly oxidized Si |
| 4 | Two-step | 300 nm for 4 h; then chemical conversion of the $PtCl_2$ headgroups | XPS results consistent with the expected monolayer composition, weakly oxidized Si, Ellipsometric thickness relatively close to that theoretically predicted |

[a] The XPS signal corresponding to the Si 2p peak was completely attenuated by the presence of the polymer layer. [b] The lower surface coverage obtained for the UV grafting of **Ptdithiolene** relative to that of **$PtCl_2$** can be reasonably ascribed to a weaker light absorption by silicon owing to the stronger absorption of the **Ptdithiolene** complex at 300 nm.

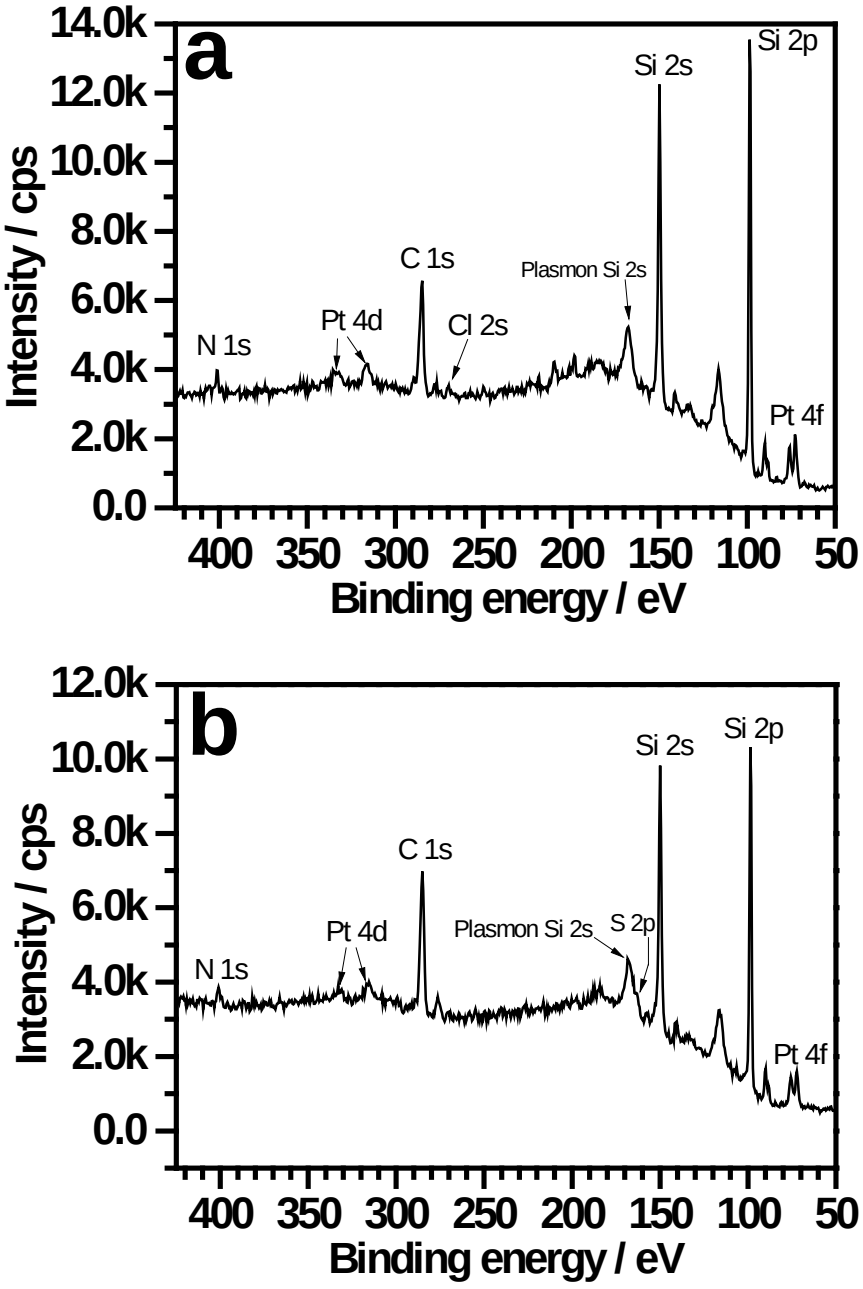


**Figure S17.** Survey XP spectra of **$PtCl_2$**- (a) and **Ptdithiolene**- (b) modified Si(111) surfaces. The peak at 276.4 eV next to the main C 1s one is a satellite peak due to the use of a non-monochromatized X-ray source.

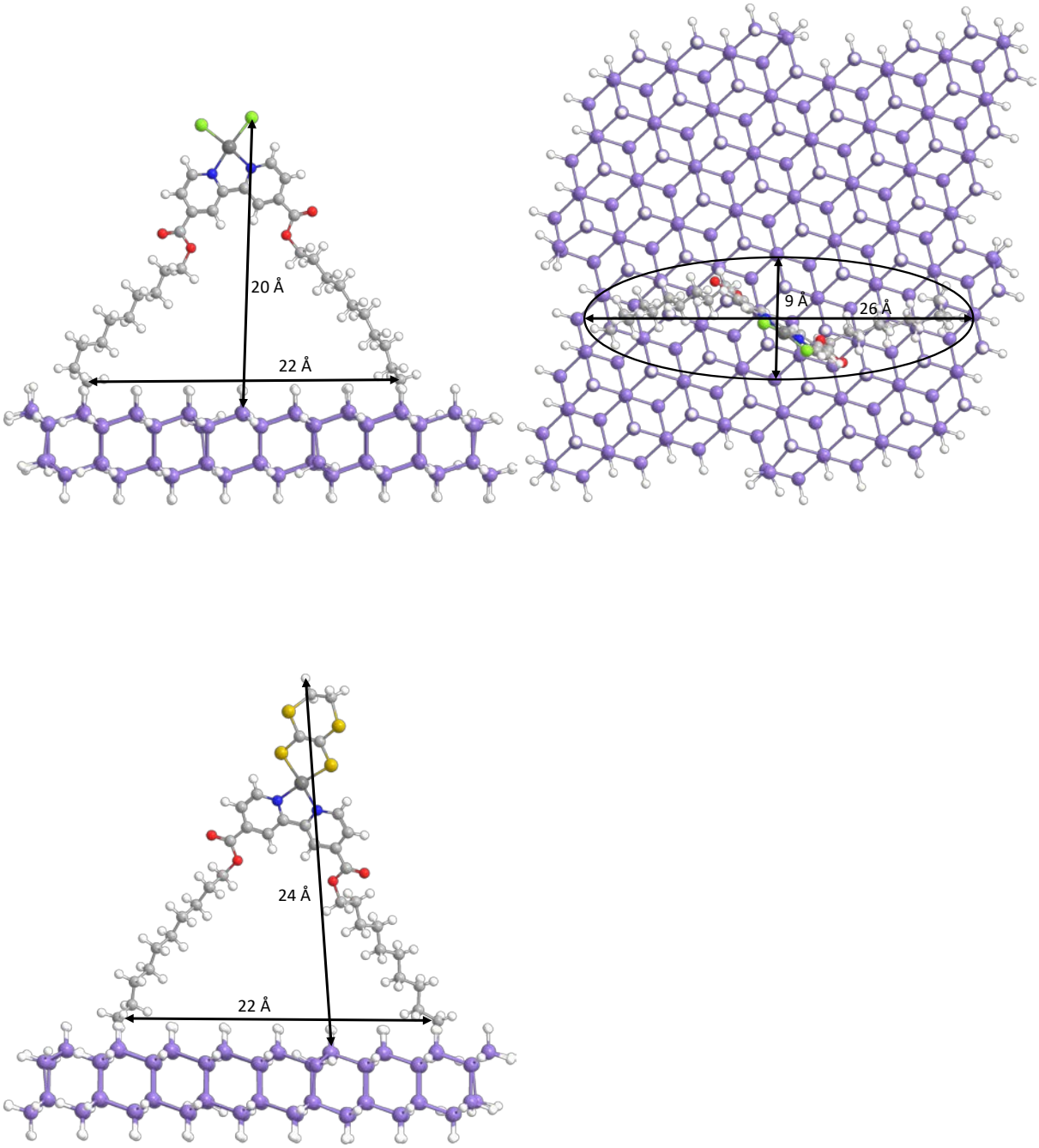


**Figure S18.** Optimized geometrical structures of Si(111)-bound **$PtCl_2$** (top) and **Pt-dithiolene** (bottom) extracted from DFT calculations, considering the two spacer arms of the molecule are strongly spread on the surface. Side (left) and top (right) views.

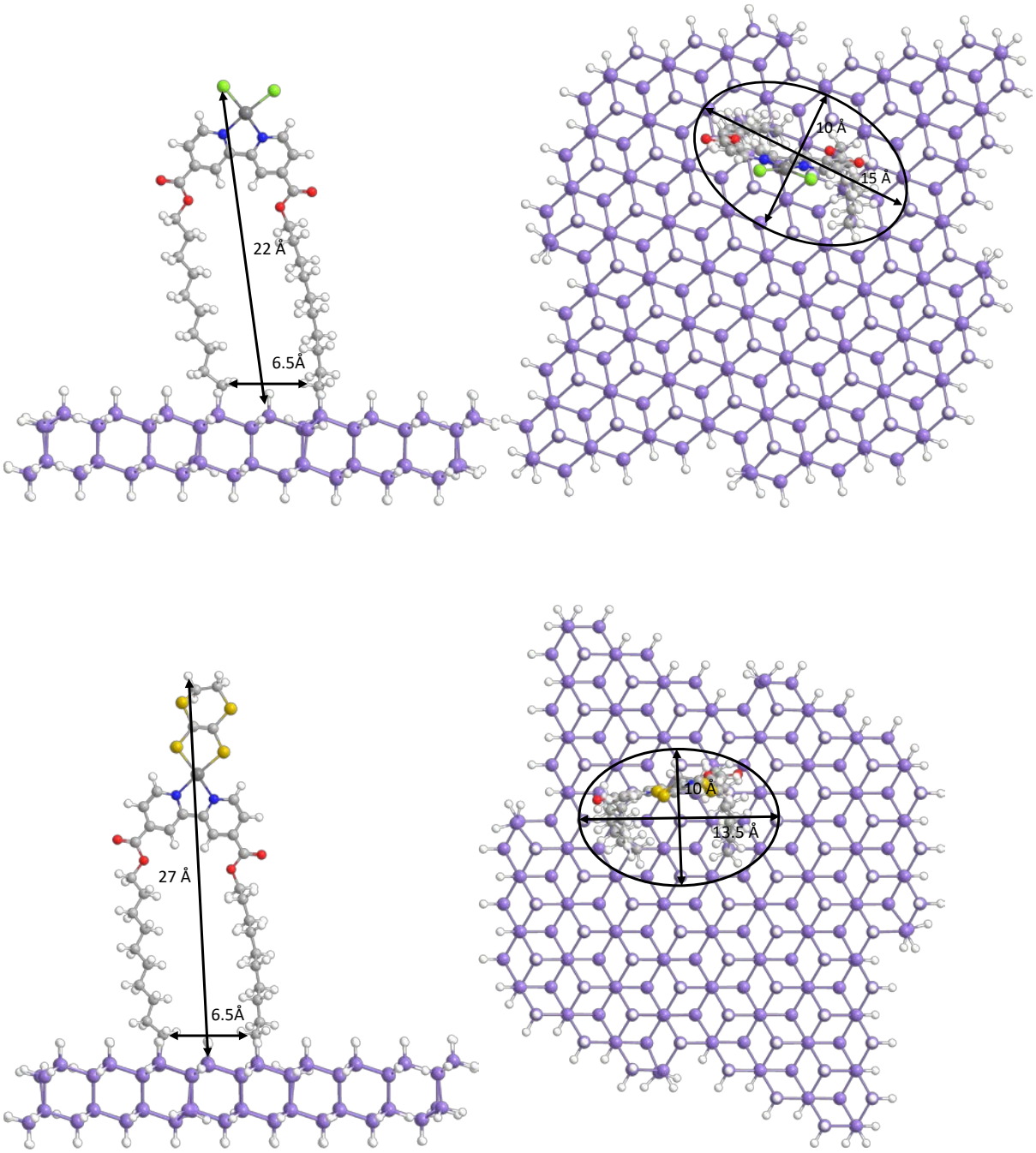


**Figure S19.** Optimized geometrical structures of Si(111)-bound **$PtCl_2$** (top) and **Pt-dithiolene** (bottom) extracted from DFT calculations, considering the two spacer arms of the molecule are closed together on the surface. Side (left) and top (right) views.

The specific area of an ellipse $A = \pi \times a \times b$ where $a$ and $b$ are the minor and major radii, respectively.

Therefore, if we assume first that the two spacer arms of the molecule are strongly spread on the surface (Figure S18), the calculated specific areas are 184 and 291 $Å^2$ per attached **$PtCl_2$** and **Pt-dithiolene**, respectively. Such values correspond to theoretical surface coverages of 5.4 x $10^{13}$ at $cm^{-2}$ (i.e. 9.0 x $10^{-11}$ mol $cm^{-2}$) and 3.4 x $10^{13}$ at $cm^{-2}$ (i.e. 5.7 x $10^{-11}$ mol $cm^{-2}$) for **$PtCl_2$** and **Pt-dithiolene**, respectively.

Now, if we assume that the two spacer arms of the molecule are closed together on the surface (Figure S19), the calculated specific areas are 118 and 106 $Å^2$ per attached **$PtCl_2$** and **Pt-dithiolene**, respectively. Such values correspond to theoretical surface coverages of 8.4 x $10^{13}$ at $cm^{-2}$ (i.e. 1.41 x $10^{-10}$ mol $cm^{-2}$) and 9.4 x $10^{13}$ at $cm^{-2}$ (i.e. 1.55 x $10^{-10}$ mol $cm^{-2}$) for **$PtCl_2$** and **Pt-dithiolene**, respectively.

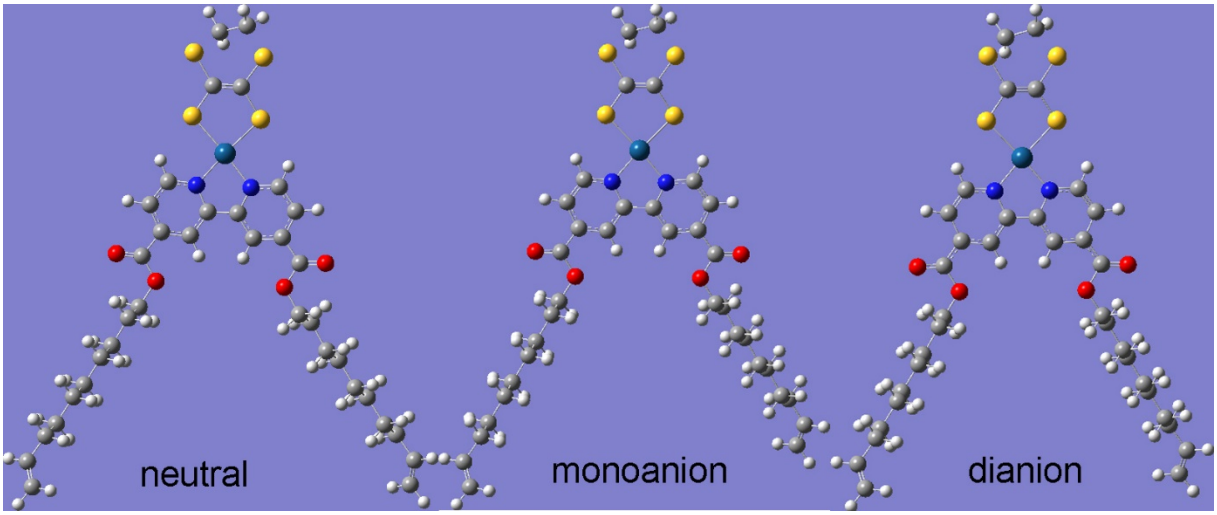


**Figure S20.** Optimized geometrical structures of the neutral, monoanionic and dianionic Ptdithiolene complexes extracted from DFT calculations.

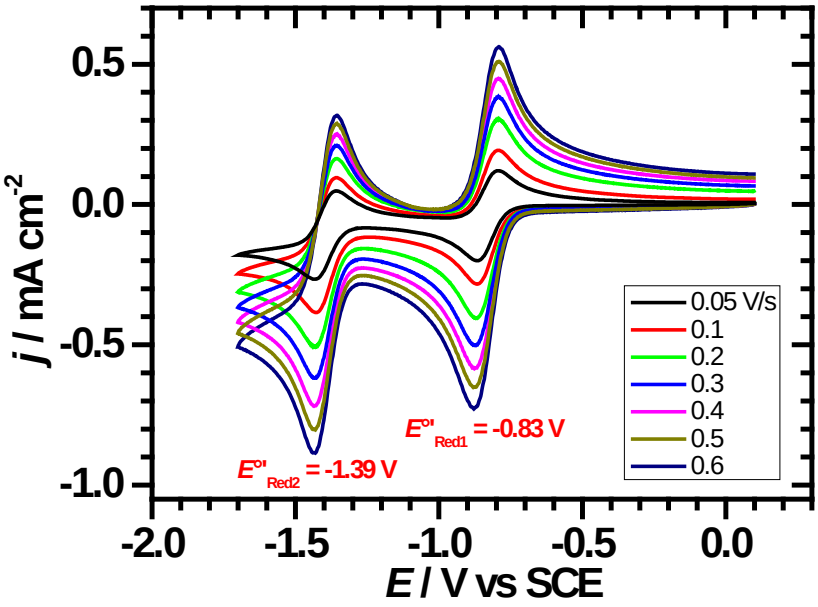


**Figure S21.** Cyclic voltammograms under argon atmosphere of **$PtCl_2$** at 1 mM in $CH_3CN$ + 0.1 M $Bu_4NClO_4$ on glassy carbon electrode.

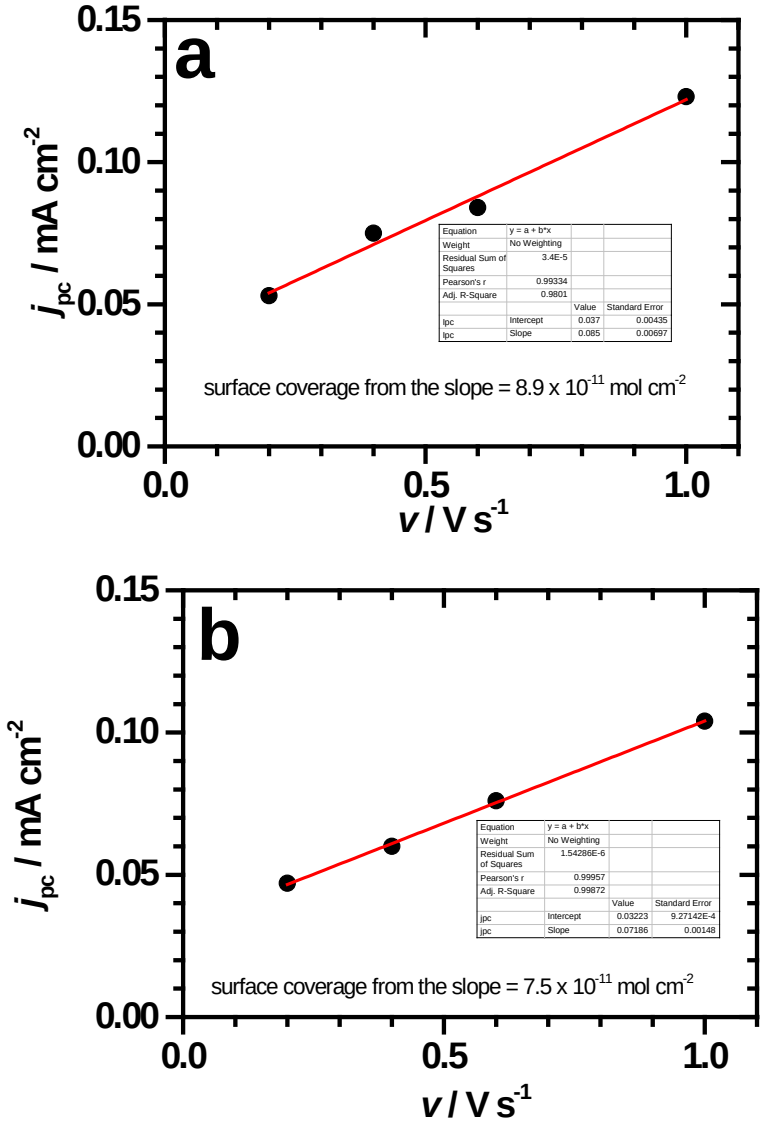


**Figure S22.** Cathodic peak photocurrent densities $j_{pc}$ (corresponding to the first redox process) vs the potential scan rate $v$ plots for **Si-PtCl$_2$** (a) and **Si-Ptdithiolene** (b). Electrolytic solution: $CH_3CN$ + 0.1 M $Bu_4NClO_4$.

The coverage surface of the Pt complex ($\Gamma$ in mol cm$^{-2}$) has been determined from the slope of the $j_{pc}$ – $v$ plot using the following equation[11]:

$$j_{pc} = \frac{n^2F^2}{4RT}\Gamma v \qquad (1)$$

where $n$ is the number of exchanged mole of electrons ($n$ = 1), $F$ is the Faraday's constant (96500 C mol$^{-1}$), $R$ is the gas constant (8.314 J K$^{-1}$ mol$^{-1}$) and $T$ is the absolute temperature (293 K).

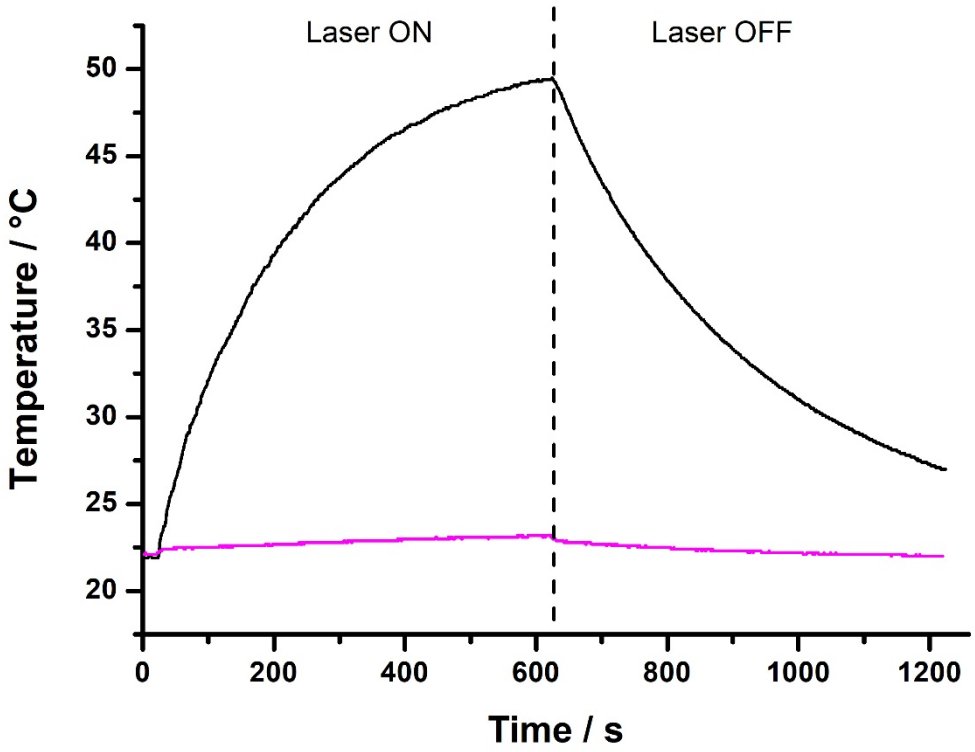


**Figure S23.** Temperature increase measured during irradiation at 808 nm of a solution of **Ptdithiolene** in toluene (C = 1 x $10^{-4}$ M) (black curve) and on pure toluene (purple curve) (1 W $cm^{-2}$, 10 min ON then 10 min OFF).

## References

(1) Roper, D.K.; Ahn, W.; Hoepfner, M. *J. Phys. Chem. C* **2007**, *111(9)*, 3636–3641.
(2) (a) Hohenberg, P; Kohn, W. *Phys. Rev.* **1964**, *136*, B864. (b) Parr, R.G.; Yang, W. *Density-Functional Theory of Atoms and Molecules*; Oxford University Press: Oxford, U.K., **1989**.
(3) (a) Becke, A.D. *Phys. Rev. A* **1988**, *38*, 3098-3100. (b) Becke, A.D. *J. Chem. Phys.* **1993**, *98*, 1372-1377. (c) Becke, A.D. *J. Chem. Phys.* **1993**, *98*, 5648-5652.
(4) C. Lee, W. Yang and R. G. Parr, *Phys. Rev. B,* 1988, **37**, 785-789.
(5) Frisch, M. J.; Trucks, G. W.; Schlegel, H. B.; Scuseria, G. E.; Robb, M. A.; Cheeseman, J. R.; Scalmani, G.; Barone, V.; Mennucci, B.; Petersson, G. A.; Nakatsuji, H.; Caricato, M.; Li, X.; Hratchian, H. P.; Izmaylov, A. F.; Bloino, J.; Zheng, G.; Sonnenberg, J. L.; Hada, M.; Ehara, M.; Toyota, K.; Fukuda, R.; Hasegawa, J.; Ishida, M.; Nakajima, T.; Honda, Y.; Kitao, O.; Nakai, H.; Vreven, T.; Montgomery, J. A., Jr.; Peralta, J. E.; Ogliaro, F.; Bearpark, M.; Heyd, J. J.; Brothers, E.; Kudin, K. N.; Staroverov, V. N.; Kobayashi, R.; Normand, J.; Raghavachari, K.; Rendell, A.; Burant, J. C.; Iyengar, S. S.; Tomasi, J.; Cossi, M.; Rega, N.; Millam, J. M.; Klene, M.; Knox, J. E.; Cross, J. B.; Bakken, V.; Adamo, C.; Jaramillo, J.; Gomperts, R.; Stratmann, R. E.; Yazyev, O.; Austin, A. J.; Cammi, R.; Pomelli, C.; Ochterski, J. W.; Martin, R. L.; Morokuma, K.; Zakrzewski, V. G.; Voth, G. A.; Salvador, P.; Dannenberg, J. J.; Dapprich, S.; Daniels,

A. D.; Farkas, Ö.; Foresman, J. B.; Ortiz, J. V.; Cioslowski, J.; Fox, D. J. Gaussian, Inc., Wallingford CT, **2009**.
(6) Bai, J.; Wei, H.; Li, B.; Song, L.; Fang, L.; Lv, Z.; Zhou, W.; Wang, E. *Chem. Asian J.* **2008**, *3*, 1935-1941.
(7) Lee, S.-K.; Shin, K.-S.; Noh, D.-Y.; Jeannin, O.; Barriere, F.; Bergamini, J.-F.; Fourmigue, M. *Chem. Asian J.* **2010**, *5*, 169-176.
(8) Price, J. H.; Birk, J. P.; Wayland, B. B. *Inorg. Chem.* **1978**, *17*, 2245-2250.
(9) Wade, C. P.; Chidsey, C. E. D. *Appl. Phys. Lett.* **1997**, *71*, 1679–1681.
(10) Sieval, A. B.; Linke, R.; Zuilhof, H.; Sudhoelter, E. J. R. *Adv. Mater.* **2000**, *12*, 1457–1460.
(11) Bard, A. J.; Faulkner, L. R. in *Electrochemical Methods: Fundamentals and Applications*, J. Wiley & Sons, **1980**, p. 522.